

PAPER • OPEN ACCESS

## Effect of ligand methylation on the spin-switching properties of surface-supported spin-crossover molecules

To cite this article: Sascha Ossinger *et al* 2020 *J. Phys.: Condens. Matter* **32** 114003

View the [article online](#) for updates and enhancements.



**IOP | ebooks™**

Bringing you innovative digital publishing with leading voices to create your essential collection of books in STEM research.

Start exploring the collection - download the first chapter of every title for free.

# Effect of ligand methylation on the spin-switching properties of surface-supported spin-crossover molecules

Sascha Ossinger<sup>1,3</sup>, Lalminthang Kipgen<sup>2,3</sup>, Holger Naggert<sup>1</sup>, Matthias Bernien<sup>2</sup>, Andrew J Britton<sup>2</sup>, Fabian Nickel<sup>2</sup>, Lucas M Arruda<sup>2</sup>, Ivar Kumberg<sup>2</sup>, Tobias A Engesser<sup>1</sup>, Evangelos Golias<sup>2</sup>, Christian Näther<sup>1</sup>, Felix Tuczek<sup>1</sup>  and Wolfgang Kuch<sup>2</sup> 

<sup>1</sup> Institut für Anorganische Chemie, Christian-Albrechts-Universität zu Kiel, Max-Eyth-Straße 2, 24118 Kiel, Germany

<sup>2</sup> Institut für Experimentalphysik, Freie Universität Berlin, Arnimallee 14, 14195 Berlin, Germany

E-mail: [kuch@physik.fu-berlin.de](mailto:kuch@physik.fu-berlin.de) and [ftuczek@ac.uni-kiel.de](mailto:ftuczek@ac.uni-kiel.de)

Received 9 September 2019, revised 22 October 2019

Accepted for publication 28 November 2019

Published 16 December 2019



## Abstract


X-ray absorption spectroscopy investigations of the spin-state switching of spin-crossover (SCO) complexes adsorbed on a highly-oriented pyrolytic graphite (HOPG) surface have shown so far that HOPG is a promising candidate to realize applications such as spintronic devices because of the stability of SCO complexes on HOPG and the possibility of highly efficient thermal and light-induced spin-state switching. Herein, we present the spin switching of several Fe(II) SCO complexes adsorbed on an HOPG surface with particular emphasis on the thermally induced spin transition behaviour with respect to different structural modifications. The complexes of the type  $[\text{Fe}(\text{bpz})_2(\text{L})]$  (bpz = dihydrobis(pyrazolyl)borate, L = 1,10-phenanthroline, 2,2'-bipyridine) and their methylated derivatives exhibit SCO in the solid state with some differences regarding cooperative effects. However, in the vacuum-deposited thick films on quartz, complete and more gradual spin transition behavior is observable via UV/vis spectroscopy. In contrast to that, all complexes show large differences upon direct contact with HOPG. Whereas the unmodified complexes show thermal and light-induced SCO, the addition of e.g. two or four methyl groups leads to a partial or a complete loss of the SCO on the surface. The angle-dependent measurement of the N K-edge compared to calculations indicates that the complete SCO and HS-locked molecules on the surface exhibit a similar preferential orientation, whereas complexes undergoing an incomplete SCO exhibit a random orientation on the surface. These results are discussed in the light of molecule-substrate interactions.

Keywords: spin-crossover complex, spin transition, physical vapor deposition, Iron(II) complex, LIESST, spin-crossover on surface, XAS



Original content from this work may be used under the terms of the [Creative Commons Attribution 3.0 licence](https://creativecommons.org/licenses/by/3.0/). Any further distribution of this work must maintain attribution to the author(s) and the title of the work, journal citation and DOI.

<sup>3</sup> These authors contributed equally to this work.

 Supplementary material for this article is available [online](#)

(Some figures may appear in colour only in the online journal)

## 1. Introduction

The two closely related spin-crossover [1–3] complexes  $[\text{Fe}(\text{bpz})_2(\text{phen})]$  (bpz = dihydrobis(pyrazolyl)borate, phen = 1,10-phenanthroline) and  $[\text{Fe}(\text{bpz})_2(\text{bipy})]$  (bipy = 2,2'-bipyridine) are (arguably) the most widely investigated SCO complexes on a surface. Over the years, only a few SCO complexes were reported to be vacuum-evaporable [4–12]. On highly-oriented pyrolytic graphite (HOPG), both molecules undergo a complete thermal- and light-induced spin transition [13–15]. On a Au(111) surface,  $[\text{Fe}(\text{bpz})_2(\text{phen})]$  decomposes into HS  $[\text{Fe}(\text{bpz})_2]$  and phenanthroline, while remaining intact and hence preserving its spin-crossover (SCO) behaviour in the second layer [4, 5]. In fact, the first observation of electric current-induced spin switching of SCO complexes—termed electron-induced excited spin-state trapping (ELIESST), in analogy to light-induced excited spin-state trapping (LIESST) [17, 18]—was made in a bilayer of  $[\text{Fe}(\text{bpz})_2(\text{phen})]$  deposited on a Au(111) surface [19]. On a Bi(111) surface, about 50% of the molecules in direct contact with the surface lose their SCO property, without any indication of molecular fragmentation [20]. This underscores the influence of the underlying substrate on the integrity and functionality of surface-adsorbed SCO complexes. On the other hand, it is a well-known phenomenon that in the solid state (bulk), the nature of spin transition of SCO complexes is highly dependent upon the chemical structure of the ligands [21]. What is of interest is to see if the SCO can similarly be tuned for SCO complexes deposited on surfaces via ligand modification. Naggert *et al.* [21] reported the tuning/modification of both the thermal- and light-induced SCO behaviour of  $[\text{Fe}(\text{bpz})_2(\text{phen})]$  by chloro- and methyl-substitutions on the phen ligand, in the bulk and in thin films. In particular,  $[\text{Fe}(\text{bpz})_2(\text{me}_2\text{-phen})]$ , i.e.  $[\text{Fe}(\text{bpz})_2(\text{phen})]$  functionalized with two methyl groups at the phenanthroline leading to 4,7-dimethyl-1,10-phenanthroline, exhibits contrasting SCO in the bulk and in the thin film: while in the former, the molecule is trapped in the HS state from 300–20 K, in the latter, the molecule undergoes both temperature- and light-induced SCO, in a manner similar to that of the parent molecule in the thin film, albeit with a slightly higher transition temperature [21].

The SCO behaviour of the molecule  $[\text{Fe}(\text{bpz})_2(\text{me}_4\text{-phen})]$ ; i.e.  $[\text{Fe}(\text{bpz})_2(\text{phen})]$  functionalized with four methyl groups on the phenanthroline leading to 3,4,7,8-tetramethyl-1,10-phenanthroline, has been investigated in the bulk as well as on Au(111) and Bi(111) surfaces [20]. The thermal-induced spin transition of  $[\text{Fe}(\text{bpz})_2(\text{me}_4\text{-phen})]$  in the bulk is rather smooth, in contrast to that of the parent molecule, which exhibits a more abrupt spin transition. However, on a Au(111) surface,  $[\text{Fe}(\text{bpz})_2(\text{me}_4\text{-phen})]$  behaves similar to the parent molecule: the molecule undergoes fragmentation into the HS  $[\text{Fe}(\text{bpz})_2]$  and (me<sub>4</sub>-phen) ligand. On a Bi(111)

surface, about 50% of the molecules lose their SCO, without any apparent indication of molecular fragmentation [20].

Herein, we report on the thermal- and light-induced SCO of the molecules  $[\text{Fe}(\text{bpz})_2(\text{me}_2\text{-phen})]$  [21],  $[\text{Fe}(\text{bpz})_2(\text{me}_4\text{-phen})]$  [20],  $[\text{Fe}(4\text{-me}_2\text{-bpz})_2(\text{phen})]$ ,  $[\text{Fe}(\text{bpz})_2(\text{me}_2\text{-bipy})]$  (me<sub>2</sub>-bipy = 4,4'-dimethyl-2,2'-bipyridine) [22],  $[\text{Fe}(\text{bpz})_2(\text{me}_4\text{-bipy})]$  (me<sub>4</sub>-bipy = 4,4',6,6'-tetramethyl-2,2'-bipyridine),  $[\text{Fe}(\text{bpz})_2(\text{tbu}_2\text{-bipy})]$  (4,4'-di-tert-butyl-2,2'-bipyridine), and  $[\text{Fe}(\text{bpz})_2(\text{dpq})]$  (dpq = dipyrido[3,2-f:2',3'-h]-quinoxaline), deposited on an HOPG surface (figure 1). The ligand dihydrobis(4-methyl-pyrazolyl)borate (4-me<sub>2</sub>-bpz) contains one methyl group per pyrazole unit (figure 1 left, dashed). The SCO behaviour of the new SCO complex  $[\text{Fe}(4\text{-me}_2\text{-bpz})_2(\text{phen})]$  is also studied in the bulk and in thin films using magnetic susceptibility measurements as well as temperature-dependent Mössbauer and UV/vis spectroscopy. The investigations of the bipy-derived molecules in the bulk and thin films are presented in the supporting information (SI) ([stacks.iop.org/JPhysCM/32/114003/mmedia](https://stacks.iop.org/JPhysCM/32/114003/mmedia)).

As will be shown in the following sections, methyl substitutions have a profound effect on the SCO behaviour of derived Fe(II) complexes upon direct contact with an HOPG surface: addition of two methyl groups to the phen or bipy ligands leads to partial SCO; addition of four methyl groups leads to complete loss of SCO. However, addition of four methyl groups to bpz ligands— $[\text{Fe}(4\text{-me}_2\text{-bpz})_2(\text{phen})]$ —results in a partial SCO.  $[\text{Fe}(\text{bpz})_2(\text{tbu}_2\text{-bipy})]$ —investigated both in the submonolayer and bilayer coverages, is also observed to undergo a partial SCO, while  $[\text{Fe}(\text{bpz})_2(\text{dpq})]$  is locked in the HS state.

For probing the molecular spin states of submonolayer or bilayer coverages on HOPG, near-edge x-ray absorption fine-structure (or simply referred to as x-ray absorption spectroscopy, XAS) is used. The high sensitivity and the element selectivity of XAS enables one to probe the spin states of the central Fe(II) ion, whereby the spectral pattern recorded at the Fe L<sub>2,3</sub>-edge (or just at the L<sub>3</sub>-edge) has a unique pattern for the HS and LS states [10, 23]. Further, XAS recorded at the N K-edge is employed to estimate the molecular orientation on HOPG surface, making use of the measured XA-intensity dependence upon the angles between the surface and the direction of the x-ray beam. For the bulk- and thin film-sample investigation of the spin states, magnetic measurements, Mössbauer and UV/vis spectroscopy are used. The spin crossover from HS to LS is accompanied by a dramatic decrease of paramagnetism down to diamagnetism (for Fe(II) compounds) due to a decrease of the number of unpaired electrons. Therefore, the magnetic susceptibility as a function of temperature ( $\chi_M T$ ) changes dramatically when the thermal spin transition temperature ( $T_{1/2}$ ) is reached [2, 24]. Temperature-dependent <sup>57</sup>Fe Mössbauer spectroscopy can also be used to probe the spin states of iron in coordination compounds as

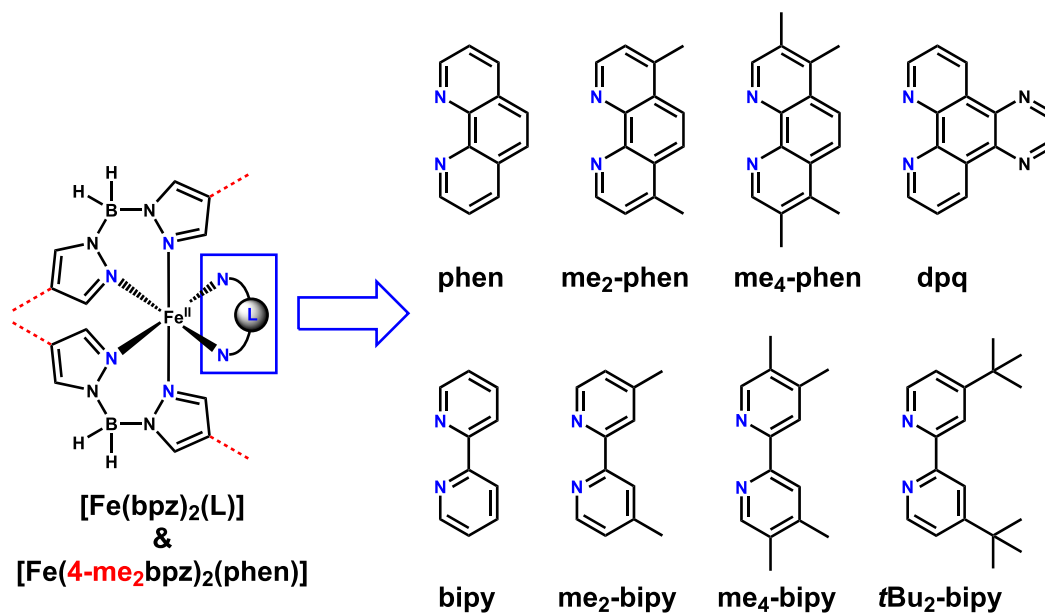


**Figure 1.** The complexes [Fe(bpz)<sub>2</sub>(L)] (black) and [Fe(4-me<sub>2</sub>bpz)<sub>2</sub>(phen)] (with red colored dotted methyl groups) investigated in this work, based on functionalized 2,2'-bipyridine, 1,10-phenanthroline and dihydrobis(pyrazolyl)borate ligands.

two of the parameters derived from the Mössbauer spectrum, i.e. the isomer shift  $\delta$  and the quadrupole splitting  $\Delta E_Q$ , vary significantly between the HS and LS state of Fe(II) [2,24]. Finally, the spin transition of SCO complexes with low-lying  $\pi^*$  orbitals of ligands with an extended  $\pi$ -system, as present in [Fe(bpz)<sub>2</sub>(phen)], can be monitored via MLCT transitions observable via UV/vis spectroscopy. Due to SCO the bands dramatically increase in the intensity from HS to LS because of the larger overlap of the metal- and ligand-orbitals which results from the shorter metal-ligand bond lengths in the LS state [2, 24].

## 2. Experimental details

### 2.1. Synthesis

K[bpz], [Fe(bpz)<sub>2</sub>(bipy)], [Fe(bpz)<sub>2</sub>(phen)], [Fe(bpz)<sub>2</sub>(me<sub>2</sub>-bipy)], [Fe(bpz)<sub>2</sub>(me<sub>2</sub>-phen)] and [Fe(bpz)<sub>2</sub>(me<sub>4</sub>-phen)] were used from or synthesized following previous studies [4, 20–22, 25–30]. The synthesis and characterisation of the new SCO complexes [Fe(4-me<sub>2</sub>bpz)<sub>2</sub>(phen)], [Fe(bpz)<sub>2</sub>(me<sub>4</sub>-bipy)], [Fe(bpz)<sub>2</sub>(tBu<sub>2</sub>-bipy)] and [Fe(bpz)<sub>2</sub>(dpq)] are described in the SI. For illumination experiments via UV/vis spectroscopy a 3 × LED Luxeon Typ LXML-PM01-0080 ( $\lambda = 519$  nm, 145 lm) from Philips Lumileds and a 1 × LED APG2C1-810 ( $\lambda = 810$  nm, 90 mW) from Roithner Lasertechnik were used.

### 2.2. X-ray absorption spectroscopy

All compounds have evaporation temperatures ranging from 150 °C to 190 °C. The samples with sub-monolayer (and multilayer) coverages on the HOPG substrate were prepared by evaporating the molecular powder from a home-made tantalum Knudsen cell onto the substrate, at a chamber pressure

of  $\sim 2 \times 10^{-8}$  mbar. The evaporation rate is monitored from the frequency change of a quartz crystal attached to the Knudsen cell. The molecular coverages were estimated from the integrated Fe L<sub>3</sub>-edge XA intensity, using the previously reported values as [13,14]. The HOPG substrate is purchased from Structure Probe, USA; a clean surface is obtained by cleaving away the top-layers using carbon tape in an auxiliary chamber maintained at a pressure of  $\sim 10^{-7}$  mbar, and valve-connected to the deposition chamber.

The XAS measurements were carried out *in-situ* at the high-field diffractometer ( $5 \times 10^{-11}$  mbar) of the beamline UE46-PGM1, the VEKMAG end-station ( $2 \times 10^{-10}$  mbar) of the beamline PM2 of BESSY II, and the group-owned end-station ( $5 \times 10^{-10}$  mbar) of the beamline UE56/2-PGM-2, of BESSY II. The photon fluxes of the beamlines are  $\sim 1 \times 10^{11}$  photons s<sup>-1</sup> cm<sup>-2</sup>,  $\sim 1.6 \times 10^{11}$  photons s<sup>-1</sup> cm<sup>-2</sup>, and  $\sim 1 \times 10^{13}$  photons s<sup>-1</sup> cm<sup>-2</sup>, respectively. The data shown in figures 4(c) and 6 originates from the high-field diffractometer end-station; figure 4(d) was recorded at the VEKMAG end-station, while figures 4(b) and 7 were recorded at the group-owned end-station. All XAS spectra are recorded by means of total electron yield—the sample drain current is recorded as a function of the x-ray photon energy and normalized to the photocurrent of a Au grid (a Pt grid in the case of PM2-VEKMAG) upstream to the experiment; the background signal from a clean HOPG substrate is also subtracted. The Fe L<sub>3</sub>-edge spectra are recorded at the so-called magic angle of 54.7° between the surface and the *k*-vector of the linearly *p*-polarized x rays; at this angle, the XA resonance intensities are independent of the orientations of the molecular orbitals on the surface. For the N K-edge spectra, the indicated angles (in figures 6 and 7) are between the *k* vector and the surface. The light-induced spin-state switching was performed with a green LED of wavelength 520 nm with a spectral width (fwhm)

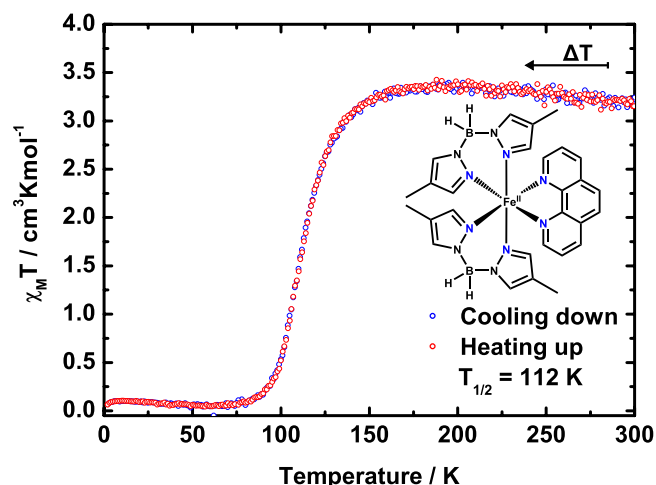


**Figure 2.**  $\chi_M T$  versus  $T$  curves of crystalline  $[\text{Fe}(4\text{-me}_2\text{-bpz})_2(\text{phen})]$  between 5 and 300 K. The curves resulting from cooling (blue symbols) and heating (red symbols) of the sample almost coincide.  $T_{1/2}$  was obtained from calculation and plot of  $\gamma_{\text{HS}}(T)$  (see SI, figure S4). Inset: Molecular structure of  $[\text{Fe}(4\text{-me}_2\text{-bpz})_2(\text{phen})]$ .

of 30 nm, with the flux density estimated to be in the range of  $4.2(8) \times 10^{14}$  photons  $\text{s}^{-1} \text{mm}^{-2}$  at the sample position.

### 3. Results and discussion

#### 3.1. Bulk properties of $[\text{Fe}(4\text{-me}_2\text{-bpz})_2(\text{phen})]$

Figure 2 shows the magnetic susceptibility of the bulk sample of  $[\text{Fe}(4\text{-me}_2\text{-bpz})_2(\text{phen})]$  as a function of temperature. The new complex shows thermal SCO with  $\chi_M T$  values ranging from  $3.15 \text{ cm}^3 \text{ K mol}^{-1}$  at 300 K to  $0.09 \text{ cm}^3 \text{ K mol}^{-1}$  at 5 K. At  $T_{1/2} = 112 \text{ K}$  (temperature where the high-spin fraction  $\gamma_{\text{HS}}$  is 50%) a fairly abrupt spin transition occurs. This behaviour is similar to other complexes of the formula  $[\text{Fe}(\text{bpz})_2(\text{L})]$  with  $\text{L} = \text{diimine}$  [4, 20–22].

The slight increase of  $\chi_M T$  with decreasing temperature prior to the spin transition can be attributed to a distinct anisotropy of the g-factor as found for another example of  $[\text{Fe}(\text{bpz})_2(\text{L})]$  compounds [22].

To obtain further information on the spin state of the iron center, Mössbauer spectra were recorded, indicating also HS at 300 K and LS at 80 K (see SI, figure S6).

#### 3.2. Vacuum Deposition of $[\text{Fe}(4\text{-me}_2\text{-bpz})_2(\text{phen})]$

$[\text{Fe}(4\text{-me}_2\text{-bpz})_2(\text{phen})]$  can be evaporated at  $180^\circ\text{C}$ ,  $p = 10^{-2}$  mbar or in an ultrahigh vacuum ( $\sim 10^{-10}$  mbar), to generate thin films on a variety of substrates. The structural integrity of the complex in these films is, e.g. evident from the fact that infrared spectra are found to be identical to those recorded from microcrystalline material [20–22]. In particular, the antisymmetric and symmetric B–H vibrations at  $\nu_{\text{asym}}(\text{B–H}) = 2393 \text{ cm}^{-1}$  and  $\nu_{\text{sym}}(\text{B–H}) = 2277 \text{ cm}^{-1}$ , respectively, are found for  $[\text{Fe}(4\text{-me}_2\text{-bpz})_2(\text{phen})]$  both in the bulk and in the vacuum-evaporated film (see SI, figure S8). Furthermore, for a film of  $[\text{Fe}(4\text{-me}_2\text{-bpz})_2(\text{phen})]$  on quartz, the metal-to-ligand charge transfer (MLCT) bands at 298 K

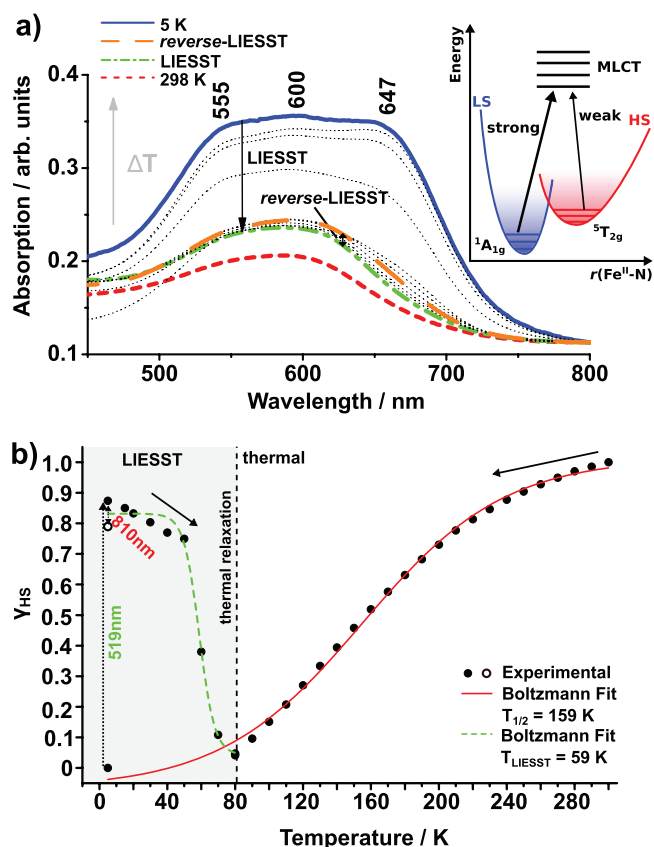


**Figure 3.** (a) Temperature-dependent UV/vis spectra of a vacuum-deposited film of compound  $[\text{Fe}(4\text{-me}_2\text{-bpz})_2(\text{phen})]$  on a quartz disk at 298 K (red dotted line) and 5 K (blue line), and LIESST at 5 K (green line; 5 min at 519 nm) and reverse-LIESST at 5 K (orange line; 15 min at 810 nm). Gray traces show spectra taken during thermal relaxation (5 to 80 K) of the LIESST state. Inset: Ground and MLCT excited states and involved transitions. (b) High-spin fraction  $\gamma_{\text{HS}}$  versus  $T$  along with Boltzmann fit (red line). The light-induced SCO at 5 K is shown by dotted black arrows (green = LIESST and orange/red = reverse-LIESST), and thermal HS-to-LS relaxation is shown by a Boltzmann fit (green dotted line).

(HS) evolve to a more intense three-band pattern centered at 555, 600 and 647 nm at 80 K (LS; figure 3 and SI, figure S10). Similar observations have been made for analogous Fe-bpz complexes, indicating thermal spin crossover from HS to LS [4, 20–22].

Importantly, vacuum-deposited films of  $[\text{Fe}(4\text{-me}_2\text{-bpz})_2(\text{phen})]$  exhibit LIESST and reverse-LIESST [17, 18]; i.e. at 5 K the low-spin state can be converted to the high-spin state by irradiation at 519 nm for 5 min and then—to a small extent - back to the low-spin state by irradiation at 810 nm for 15 min (figure 3(a)). As the intensity of the MLCT band differs in the HS and the LS state (see figure 3(a)), it can be taken to monitor the spin transition. In figure 3(b), the high-spin fraction  $\gamma_{\text{HS}}$  derived from the intensity of the MLCT band is displayed versus the temperature [4, 20, 21]. The thermal transition is significantly more gradual than in the solid state (see figure 2), presumably due to weaker cooperative effects in the vacuum-deposited film. Moreover, the thermal spin transition temperature  $T_{1/2}$  of 159 K is significantly higher than in the bulk material (see above). Finally, the critical temperature for



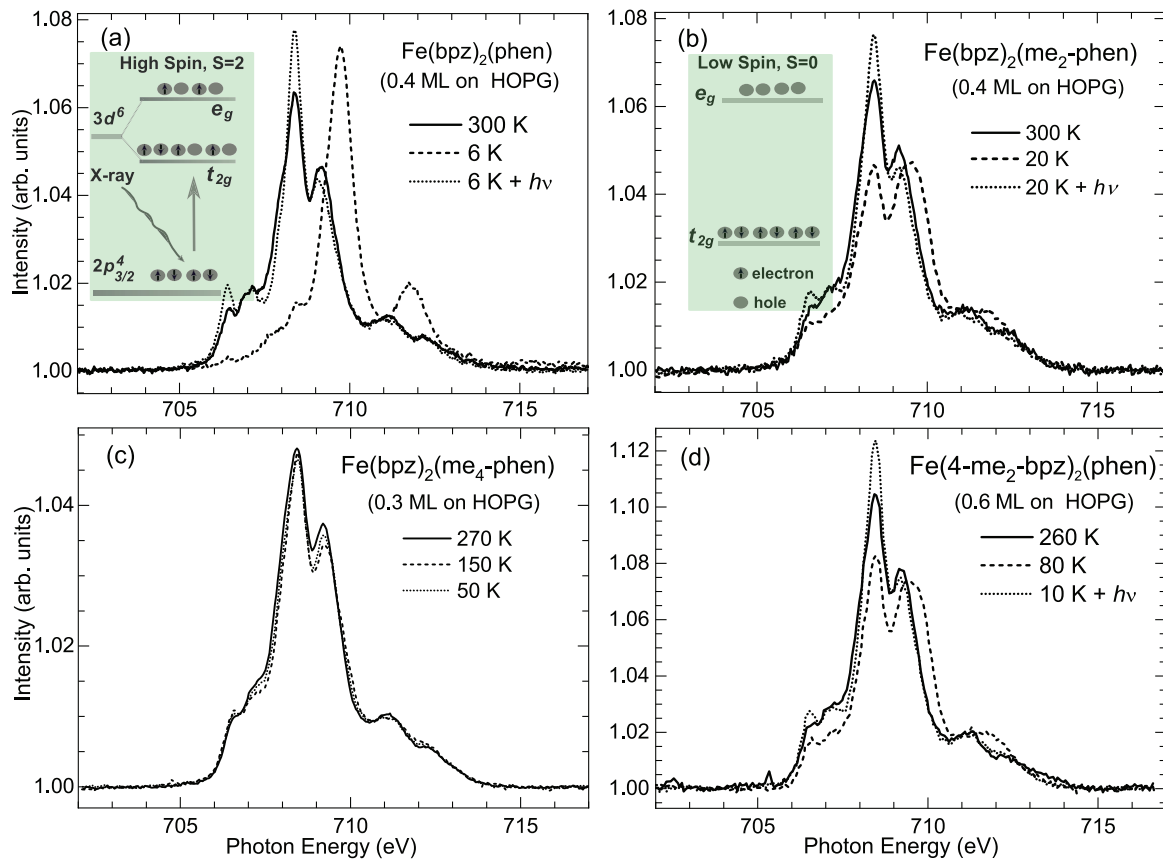


**Figure 4.** Fe  $L_3$ -edge XA spectra of: (a) 0.4 ML of  $[\text{Fe}(\text{bpz})_2(\text{phen})]$  on HOPG; (b) 0.4 ML of  $[\text{Fe}(\text{bpz})_2(\text{me}_2\text{-phen})]$  on HOPG; (c) 0.3 ML of  $[\text{Fe}(\text{bpz})_2(\text{me}_4\text{-phen})]$  on HOPG, and (d) 0.6 ML of  $[\text{Fe}(4\text{-me}_2\text{-bpz})_2(\text{phen})]$  on HOPG. Spectra in (a) have already been published in [13]. The inset of (a) shows the high-spin configuration where electrons occupy both the  $e_g$  and  $t_{2g}$  levels, while the inset of (b) shows the low-spin configuration where the lower  $t_{2g}$  level is fully occupied by electrons.

the HS-to-LS relaxation is  $T_{\text{LIESST}} = 59$  K. The other vacuum-deposited films exhibit similar properties (see SI; figure S13).

### 3.3. XA spectroscopy in submonolayers on graphite surfaces

The x-ray absorption spectroscopy recorded at the Fe  $L_3$ -edge has been reported—and is well-documented by now—to be a good indicator of the spin states of SCO molecules [13, 14, 23]. As an example, figure 4(a) shows the Fe  $L_3$ -edge—reproduced from [13]—of 0.4 monolayer (ML) of  $[\text{Fe}(\text{bpz})_2(\text{phen})]$  on an HOPG surface, undergoing a complete spin-state switching induced by temperature and light.

The molecule in the HS state at 300 K is characterized by two main peaks at 708.4 and 709.1 eV, while the LS state at 6 K is characterized by a single main peak at 709.7 eV (solid and dashed lines, respectively). On illumination with green light at 6 K, the molecule switches to the HS state, as indicated by the resultant spectral pattern (dotted line, figure 4(a)) similar to that recorded at 300 K.

The spectral patterns of the HS and LS states can be explained within the framework of a one-electron model as: the presence of holes at both the  $e_g$  and  $t_{2g}$  levels in the HS configuration—depicted in the inset of figure 4(a)—accounts for the double-peak feature of the HS spectrum; while the presence of holes only at the  $e_g$  level in the LS configuration—as depicted in the inset of figure 4(b)—accounts for

the single-peak feature of the LS spectrum. A realistic understanding of the spectral patterns is possible within the atomic multiplet calculations, which take into account the multi-electron nature of the initial and final states [13, 31].

Figure 4(b) shows the Fe  $L_3$ -edge XA spectra of about 0.4 ML of  $[\text{Fe}(\text{bpz})_2(\text{me}_2\text{-phen})]$  on an HOPG surface, recorded at 300 K (solid line), at 20 K and also at 20 K after illumination with a green LED for about 10 min (dashed and dotted lines). While the spectra at 300 K and at 20 K after illumination indicate the HS state of the molecule—similar to that of the parent molecule of figure 4(a)—the spectrum at 20 K before illumination with light shows both the HS and LS peaks at 708.4 and 709.7 eV, respectively. The spin-state composition at 20 K of the sample can be estimated by a linear combination of the HS and LS spectra of the parent molecule  $[\text{Fe}(\text{bpz})_2(\text{phen})]$  given in figure 4(a); by this procedure, the HS fraction is estimated to 65(5)% at 20 K. In contrast, the complex  $[\text{Fe}(\text{bpz})_2(\text{me}_2\text{-phen})]$  in the solid state (bulk) is reported to be trapped in the HS state from 300 K down to 20 K [21].

On adding four methyl groups to the phen ligand, i.e. in  $[\text{Fe}(\text{bpz})_2(\text{me}_4\text{-phen})]$ , the molecule loses its SCO property and is trapped in the HS state from 300 K down to low temperatures on an HOPG surface; this is shown in figure 4(c) for a coverage of 0.3 ML. This contrasts sharply with the SCO behaviour of the bulk molecule, which is reported to undergo

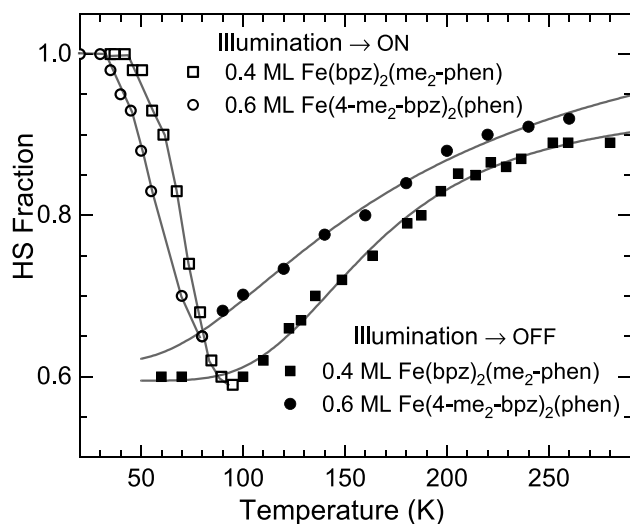


**Figure 5.** Thermal-induced SCO of 0.4 ML of  $[\text{Fe}(\text{bpz})_2(\text{me}_2\text{-phen})]$  (squares) and 0.6 ML of  $[\text{Fe}(4\text{-me}_2\text{-bpz})_2(\text{phen})]$  (circles) on HOPG. The open and solid circles (and squares) represent, respectively, the spin transition with and without light exposure. Solid lines are guides to the eyes.

both temperature- and light-induced SCO, in a manner quite similar to the parent, non-methylated molecule [20].

The implementation of methyl groups to the bpz ligand in the complex  $[\text{Fe}(4\text{-me}_2\text{-bpz})_2(\text{phen})]$  changes the SCO behaviour on a HOPG surface less than methylation of the phen ligand. Nevertheless, the complex undergoes only a partial spin switching upon contact with an HOPG surface, unlike the thin film and bulk samples that exhibit a complete thermal- and light-induced SCO. This is shown in figure 4(d) for 0.6 ML of  $[\text{Fe}(4\text{-me}_2\text{-bpz})_2(\text{phen})]$ ; HS state at 260 K (solid lines), and a minimum HS fraction of about 60(5)% recorded at 80 K (dashed lines). On illumination with a green LED for about 10 min, the sample is converted to the HS state (figure 4(d), dotted spectrum).

The temperature dependence of the high-spin fractions of  $[\text{Fe}(\text{bpz})_2(\text{me}_2\text{-phen})]$  and  $[\text{Fe}(4\text{-me}_2\text{-bpz})_2(\text{phen})]$  on HOPG is shown in figure 5; the cooling curves from around 300 K to 50–70 K are indicated by solid points (solid squares and solid dots for the  $[\text{Fe}(\text{bpz})_2(\text{me}_2\text{-phen})]$  and  $[\text{Fe}(4\text{-me}_2\text{-bpz})_2(\text{phen})]$  samples, respectively). The open dots and open squares represent the relaxation of the molecules from the light-induced HS state generated at 10–20 K to the LS state on raising the temperature to 100 K.

Similar SCO behaviour is also observed for the closely related complex,  $[\text{Fe}(\text{bpz})_2(\text{bipy})]$ , on ligand-methylation and upon contact with an HOPG surface; this is shown in figure 6 for the complexes  $[\text{Fe}(\text{bpz})_2(\text{me}_2\text{-bipy})]$  and  $[\text{Fe}(\text{bpz})_2(\text{tbu}_2\text{-bipy})]$ , each deposited in coverage of about 0.5 ML. In figure 6, the SCO behaviour of a bilayer sample of  $[\text{Fe}(\text{bpz})_2(\text{tbu}_2\text{-bipy})]$  on HOPG is also shown. It is obvious that the thermal-induced spin-state transition for the bilayer sample is more complete as compared to the submonolayer sample—minimum HS fraction of about 44(5)% and 61(5)% at 60 K, respectively—indicating the role of the surface in constraining/impeding the SCO behaviour of SCO complexes.

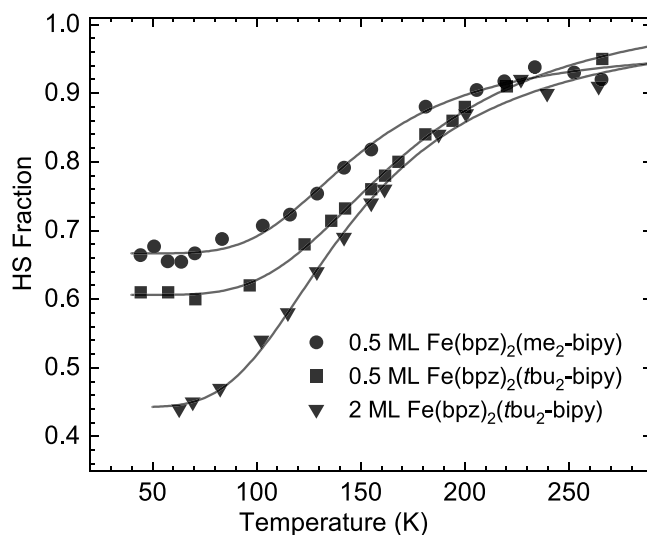


**Figure 6.** Thermal-induced SCO of 0.5 ML of  $[\text{Fe}(\text{bpz})_2(\text{me}_2\text{-bipy})]$  (solid circles);  $[\text{Fe}(\text{bpz})_2(\text{tbu}_2\text{-bipy})]$  of 0.5 ML and 2 ML (solid squares and solid triangles, respectively) on HOPG. Solid lines are guides to the eyes.

$[\text{Fe}(\text{bpz})_2(\text{me}_4\text{-bipy})]$  and  $[\text{Fe}(\text{bpz})_2(\text{dpq})]$  of submonolayer coverages on HOPG are locked in the HS state; the spectra are given in the SI (figure S14).

The utility of the N K-edge in probing the stability of  $[\text{Fe}(\text{bpz})_2(\text{phen})]$  upon contact with a gold surface has been reported earlier [16, 20]. Notably, the XA intensity depends upon the relative orientation between the  $k$ -vector and the  $\text{N}-\pi^*$ -orbitals of the complex (figure 7). This will be used to probe the preferential orientation (and also the integrity) on the HOPG surface of the complex  $[\text{Fe}(\text{bpz})_2(\text{phen})]$  and its derivatives  $[\text{Fe}(\text{bpz})_2(\text{me}_2\text{-phen})]$ ,  $[\text{Fe}(\text{bpz})_2(\text{me}_4\text{-phen})]$  as well as the closely related  $[\text{Fe}(\text{bpz})_2(\text{bipy})]$  complex (figure 8). Corresponding data for  $[\text{Fe}(\text{bpz})_2(\text{me}_2\text{-bipy})]$  and  $[\text{Fe}(\text{bpz})_2(\text{tbu}_2\text{-bipy})]$  are given in the SI. The N atoms of  $[\text{Fe}(\text{bpz})_2(\text{phen})]$  can be grouped into three types, based on their position: #1 from the two N atoms of phen ligands; #2 from the four inner N atoms of the bpz ligands in direct coordination with the central Fe(II) ion; and #3 from the four outer N atoms from the bpz ligands. This is shown in the inset of figure 8(a).

Figures 8(a)–(c) show, respectively, the N K-edge XA of submonolayers of  $[\text{Fe}(\text{bpz})_2(\text{phen})]$ ,  $[\text{Fe}(\text{bpz})_2(\text{me}_4\text{-phen})]$  and  $[\text{Fe}(\text{bpz})_2(\text{bipy})]$  recorded at 25° (solid lines) and 90° angles (dotted lines) between the  $k$ -vector of the x-ray beam and the HOPG surface. Importantly, all the samples showed identical spectral patterns—with similar XA intensities at the peaks #1 at 399.1 eV, #2 at 400.8 eV, #3 at 401.3 eV. The peaks marked #1, #2 and #3 in figure 8 correspond to transitions to the  $\pi^*$ -antibonding orbitals of the three respective classes of N atoms of the SCO molecules. The broad peaks at the higher energies (>405 eV) are due to transitions to the  $\sigma^*$ -antibonding orbitals. The difference in the XA intensity of the spectra recorded at 25° and 90° angles reflect the preferential orientation—as opposed to a random one—of the above-mentioned complexes on the HOPG surface. In particular, the higher intensity for the peak marked #1 at 25° is due to the

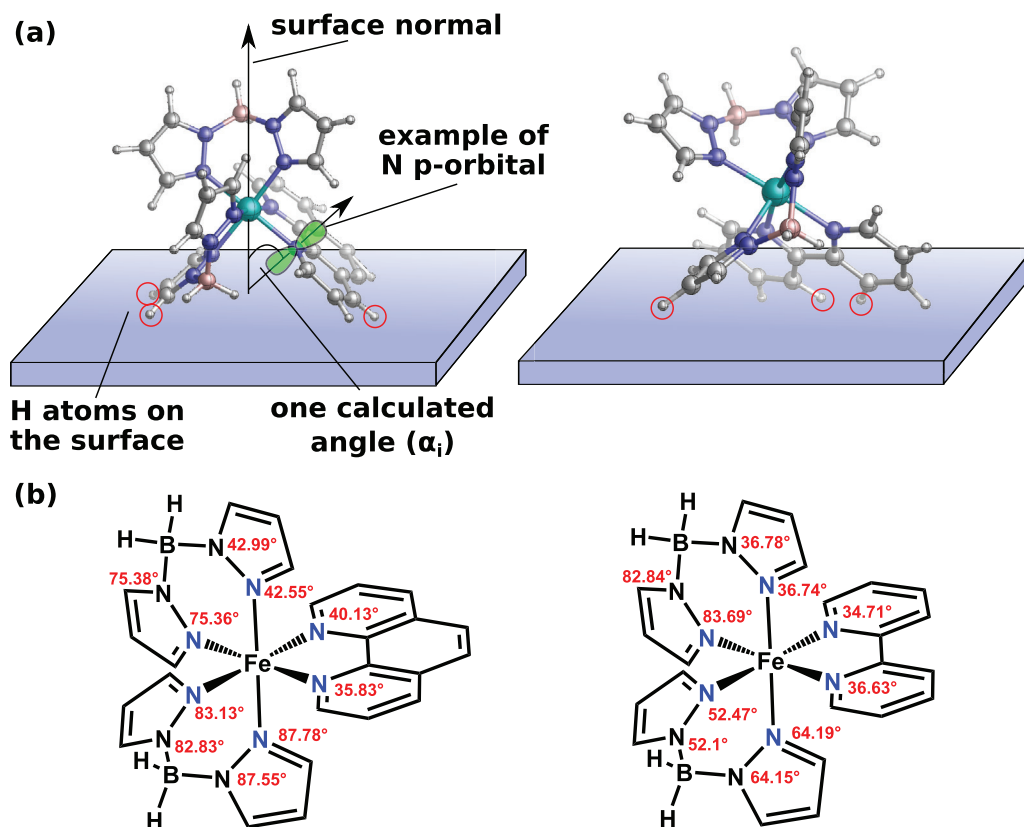


**Figure 7.** Assumed orientation (a) of the complex  $[\text{Fe}(\text{bpz})_2(\text{phen})]$  (left) and  $[\text{Fe}(\text{bpz})_2(\text{bipy})]$  (right) for the calculations of the expected intensity ratio for a non-distorted system in direct contact with a graphite surface. H atoms marked with red circles are standing on the surface and one of the N p-orbitals marked in green. The black arrows present the calculated orthogonal vectors and the marked angle is an example of one of the calculated angles  $\alpha_i$ , which are presented in (b) for the complexes  $[\text{Fe}(\text{bpz})_2(\text{phen})]$  (left) and  $[\text{Fe}(\text{bpz})_2(\text{bipy})]$  (right).

greater overlap of the  $\pi^*$ -antibonding orbitals of #1 N-atoms to the  $k$ -vector of the x-ray beam than at  $90^\circ$ . But in the case of the peaks #2 and #3, the reverse is true.

For the orientation and geometry of the molecules in direct contact with the graphite surface we assumed a non-distorted geometry similar to the discrete complex in the crystal structure of  $[\text{Fe}(\text{bpz})_2(\text{phen})]$  and  $[\text{Fe}(\text{bpz})_2(\text{bipy})]$ . The complexes should stand with at least three H atoms from one pyrazole ring and the co-ligand phen or bipy on the surface (figure 7(a)). This orientation is similar to that of  $[\text{Fe}(\text{bpz})_2(\text{phen})]$  in the second layer on Au(111) proposed by Gopakumar *et al* [19]. The assumed orientation was used for the calculation of the theoretical transition dipole moment orientations and expected intensity ratios ( $R = I_{\text{grazing}}/I_{\text{normal}}$ ). Comparison with the measured values given in figure 8 should confirm or disprove the assumed orientation. The angle of the p-orbital on each N atom was determined from the undistorted molecular structure. It was thereby assumed that due to rotational distribution of the molecules all corresponding angles are arranged on a cone around the surface normal (figure 7(b) and see SI).

The values of the experimental and calculated intensity ratios  $R$  match well (Table 1). For  $[\text{Fe}(\text{bpz})_2(\text{phen})]$  the intensity ratios of the respective groups #1  $R = 2.707$ , #2  $R = 0.53$  and #3  $R = 0.5231$  were calculated in good agreement with the experimental values (#1  $R = 2.461$ , #2  $R = 0.55$  and #3  $R = 0.5877$ ). The calculated values for  $[\text{Fe}(\text{bpz})_2(\text{bipy})]$  are #1  $R = 3.37$ , #2  $R = 0.90$  and #3  $R = 0.90$ , while the

experimental values are #1  $R = 2.82$ , #2  $R = 0.705$  and #3  $R = 0.73$ . Finally, for  $[\text{Fe}(\text{bpz})_2(\text{me}_4\text{-phen})]$  no  $R$  values could be predicted as no crystal structure is available. However, also for this molecule  $R$  values close to those of the parent compound  $[\text{Fe}(\text{bpz})_2(\text{phen})]$  are experimentally determined. Altogether, these three complexes investigated by N K-edge NEXAFS (figure 8) thus show no significant differences in the experimental intensity ratios. The relatively good agreement between calculated and experimental values (table 1) indicates that these three complexes probably stand in the proposed, almost undistorted orientation on a graphite surface.

As already mentioned,  $[\text{Fe}(\text{bpz})_2(\text{phen})]$  and  $[\text{Fe}(\text{bpz})_2(\text{bipy})]$  exhibit complete SCO with temperature and light on an HOPG surface [13, 14]. Therefore, it is not surprising that both retain their molecular geometry (octahedral symmetry) on the surface—a basic requirement for the observance of the SCO phenomenon. What is surprising, however, is the complete loss of SCO properties of  $[\text{Fe}(\text{bpz})_2(\text{me}_4\text{-phen})]$ , although the N K-edge spectra of figure 8(b) indicate that these molecules retain both, the molecular integrity and the octahedral symmetry on the HOPG surface.

For the molecule  $[\text{Fe}(\text{bpz})_2(\text{me}_2\text{-phen})]$ , which exhibits a partial thermal-induced spin transition on HOPG, the N K-edge spectra recorded at two different angles ( $25^\circ$  and  $90^\circ$ ) between the  $k$ -vector of the x-ray beam and the HOPG surface are shown in figure 9 for two different coverages: 0.4 ML (a) and 4 ML (b). The XA intensities for both angles in all the



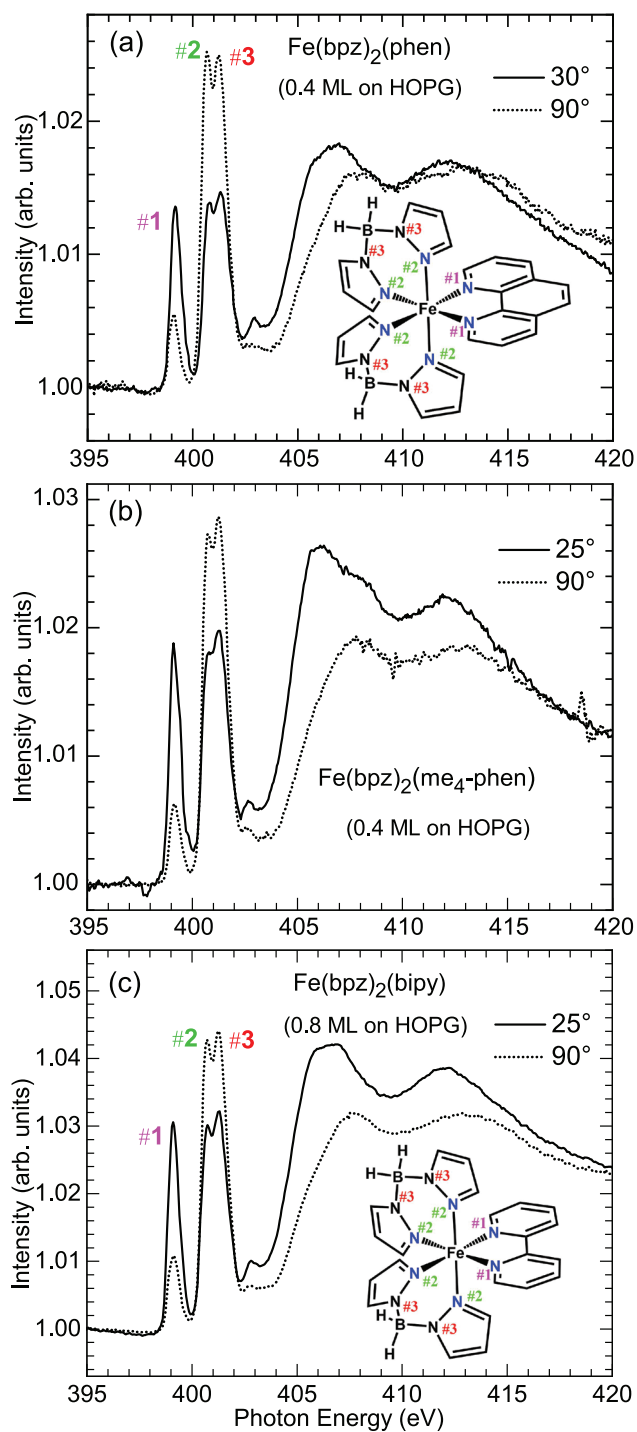


**Figure 8.** N K-edge spectra recorded at grazing (solid lines) and normal (dots) angles between the x-ray beam and the HOPG surface of: (a) 0.4 ML of  $[\text{Fe}(\text{bpz})_2(\text{phen})]$ ; (b) 0.4 ML of  $[\text{Fe}(\text{bpz})_2(\text{me}_4\text{-phen})]$ ; and (c) 0.8 ML of  $[\text{Fe}(\text{bpz})_2(\text{bipy})]$ . #1, #2 and #3 are the resonances corresponding to the N atoms as indicated in the inset.

three peaks are approximately the same. The 4-ML sample is expected to be amorphous, and as such, its N K-edge spectra shown in figure 9(b) would indicate a random orientation of the molecules, irrespective of the molecular geometry. The N K-edge XA spectral pattern of the 0.5-ML sample, as shown in figure 9(a), is also independent of the angle, indicating a random distribution of the molecules on the surface—much

**Table 1.** Comparison of the calculated and experimentally obtained intensity ratios ( $R = I_{\text{grazing}}/I_{\text{normal}}$ ) for the three groups of N-atoms.

Complex	#1 R	#2 R	#3 R
$[\text{Fe}(\text{bpz})_2(\text{phen})]$ —calc.	2.707	0.53	0.5231
Exp.	2.461	0.55	0.5877
$[\text{Fe}(\text{bpz})_2(\text{bipy})]$ —calc.	3.37	0.90	0.90
Exp.	2.82	0.705	0.73
$[\text{Fe}(\text{bpz})_2(\text{me}_4\text{-phen})]$ —Calc.	/	/	/
Exp.	2.93	0.662	0.6907

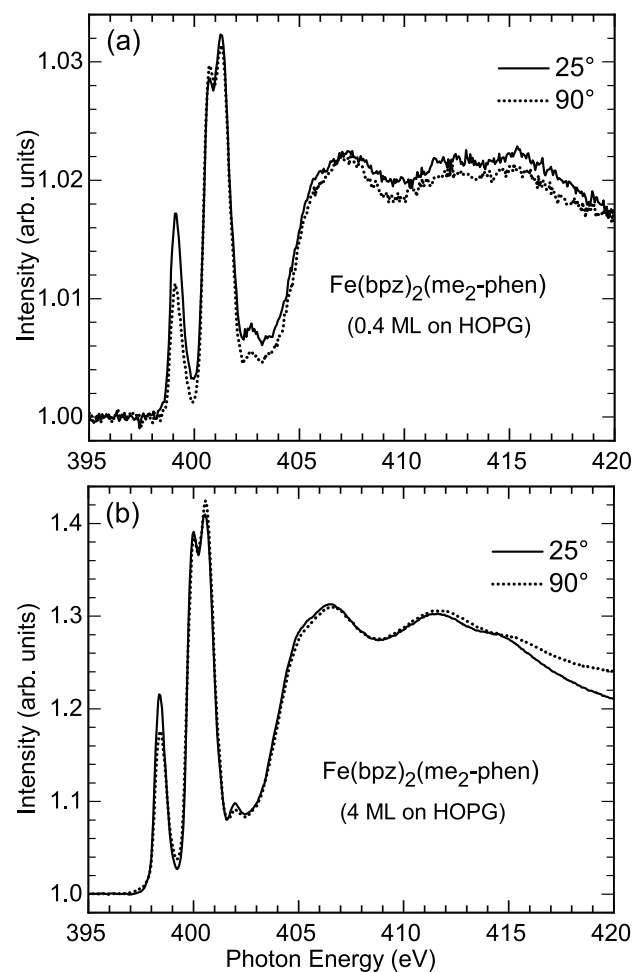


**Figure 9.** N K-edge spectra recorded at 25° (solid lines) and 90° (dots) angles between the x-ray beam and the HOPG surface of: (a) 0.4 ML of  $[\text{Fe}(\text{bpz})_2(\text{me}_2\text{-phen})]$ ; (b) 4 ML of  $[\text{Fe}(\text{bpz})_2(\text{me}_2\text{-phen})]$ .

like the multi-layered amorphous sample of figure 9(b). Notably, the N K-edge XA spectra of  $[\text{Fe}(\text{bpz})_2(\text{me}_2\text{-bipy})]$  (0.5 ML) and  $[\text{Fe}(\text{bpz})_2(\text{tbu}_2\text{-bipy})]$  (0.5 and 2 ML)—both exhibiting an incomplete thermal-induced SCO, figure 6—also show similar pattern to that shown in figure 9 (figure S16 of SI).

The partial spin crossover or the coexistence of both the spin states for SCO molecules in direct contact with a solid surface is quite a common phenomenon [7, 16, 32–34], attributed to the molecule–substrate interactions.

In particular, in an STM-based investigation of  $[\text{Fe}(\text{1,10-phenanthroline})_2(\text{NCS})_2]$  on the Cu(100) surface with coverage ranging from single molecules to bilayers [35], the specific absorption sites are found to determine the spin state (HS or LS) of the molecule—some sites favouring the HS state, and yet others favouring the LS state. In a recent investigation of a monolayer of an SCO molecule  $[\text{Fe}^{\text{II}}((3,5\text{-CH}_3)_2\text{pz})_3\text{BH}_2]$  deposited on a Au(111) surface—and apart from establishing the epitaxial relationship between the molecule and the surface using x-ray diffraction—the authors established that, indeed, mixed spin states are favoured for SCO complex-substrate systems, and their interaction energy (epitaxial strain energy) as being responsible for stabilizing a certain proportion of HS molecules at low temperatures—using DFT calculation and a mechanoelastic model [36].

#### 4. Conclusions

The combined Fe  $L_3$ -edge and N K-edge NEXAFS studies revealed that the SCO complexes undergoing a complete temperature- and light-induced SCO on an HOPG surface, namely  $[\text{Fe}(\text{bpz})_2(\text{phen})]$  and  $[\text{Fe}(\text{bpz})_2(\text{bipy})]$ , exhibit a preferred orientation on the surface in which the molecules stand with one pyrazole ring and phen/bipy on the surface. Importantly, the addition of methyl groups to the parent SCO complexes always results in a partial or a complete loss of the SCO (see SI, table S3). N K-edge XA spectra of the methylated complexes indicate that the addition of methyl groups leads to two different classes of molecules. In the case of  $[\text{Fe}(\text{bpz})_2(\text{me}_4\text{-phen})]$  on the HOPG surface, the molecule shows an orientation and a geometry similar to the parent molecule, but the complex is HS-locked, probably due to  $\text{CH}-\pi$  interactions between the methyl groups and HOPG [37]. In contrast to that, the complexes  $[\text{Fe}(\text{bpz})_2(\text{me}_2\text{-phen})]$ ,  $[\text{Fe}(\text{bpz})_2(\text{me}_2\text{-bipy})]$  and  $[\text{Fe}(\text{bpz})_2(\text{tbu}_2\text{-bipy})]$ —all undergoing incomplete SCO on HOPG—show a random orientation on the surface. The most simple rationalization of these findings would be that these molecules exhibit at least two different orientations, one that shows SCO and another which is HS-locked—probably in a similar orientation such as the parent systems and  $[\text{Fe}(\text{bpz})_2(\text{me}_4\text{-phen})]$ —leading in total to an incomplete SCO on HOPG. While the introduction of methyl groups thus may enhance the SCO complexes–HOPG interactions for this class of molecules as well, the N K-edge NEXAFS spectra clearly show that this also occurs without causing any observable molecular distortions.

#### Acknowledgments

Financial support by the Deutsche Forschungsgemeinschaft (DFG) through SFB 658, SFB 677 and SFB/TRR 227 is gratefully acknowledged.


We thank the Helmholtz-Zentrum Berlin (HZB) for the allocation of synchrotron radiation beamtime. The x-ray absorption measurements were carried out at the beamlines UE46-PGM1 (end-station: High-field diffractometer), PM2-VEKMAG (end-station: VEKMAG), and UE56-2/PGM-2

(end-station: Home-built UHV chamber), of BESSY II, HZB. We thank E Schierle, E Weschke, C Luo, H Ryll, F Radu, B Zada and W Mahler for their technical support during the beamtimes. LMA acknowledges funding from CAPES (No. 9469/13-3) and Dahlem Research School, Freie Universität Berlin.

We thank S Pehlke and J Pick for vibrational spectroscopy and CHNS measurements, D Meyer for ESI mass spectrometry measurements, H Lühmann and M Rasmussen for magnetic measurements, T Neumann for XRPD and I Jeß for x-ray single crystal measurements.

#### ORCID iDs

Felix Tuczek  <https://orcid.org/0000-0001-7290-9553>

Wolfgang Kuch  <https://orcid.org/0000-0002-5764-4574>

#### References

- [1] Gütlich P, Garcia Y and Goodwin H A 2000 Spin crossover phenomena in Fe(II) complexes *Chem. Soc. Rev.* **29** 419–27
- [2] Gütlich P, Gaspar A B and Garcia Y 2013 Spin state switching in iron coordination compounds *Beilstein J. Org. Chem.* **9** 342–91
- [3] Gütlich P, Hauser A and Spiering H 1994 Thermal and optical switching of iron(II) complexes *Angew. Chem., Int. Ed. Engl.* **33** 2024–54
- [4] Naggert H, Bannwarth A, Chemnitz S, von Hofe T, Quandt E and Tuczek F 2011 First observation of light-induced spin change in vacuum deposited thin films of iron spin crossover complexes *Dalton Trans.* **40** 6364–6
- [5] Shi S *et al* 2009 Study of molecular spin-crossover complex  $\text{Fe}(\text{phen})_2(\text{NCS})_2$  thin films *Appl. Phys. Lett.* **95** 043303
- [6] Bairagi K *et al* 2018 Temperature-, light-, and soft x-ray-induced spin crossover in a single layer of Fe II-pyrazolylborate molecules in direct contact with gold *J. Phys. Chem. C* **122** 727–31
- [7] Bairagi K *et al* 2016 Molecular-scale dynamics of light-induced spin cross-over in a two-dimensional layer *Nat. Commun.* **7** 12212
- [8] Mahfoud T, Molnar G, Cobo S, Salmon L, Thibault C, Vieu C, Demont P and Bousseksou A 2011 Electrical properties and non-volatile memory effect of the  $[\text{Fe}(\text{HB}(\text{pz})_3)_2]$  spin crossover complex integrated in a microelectrode device *Appl. Phys. Lett.* **99** 53307
- [9] Shalabaeva V, Rat S, Manrique-Juarez M D, Bas A-Ci, Vendier L, Salmon L, Molnár G and Bousseksou A 2017 Vacuum deposition of high-quality thin films displaying spin transition near room temperature *J. Mater. Chem. C* **5** 4419–25
- [10] Bernien M, Wiedemann D, Hermanns C F, Krüger A, Rolf D, Kroener W, Müller P, Grohmann A and Kuch W 2012 Spin crossover in a vacuum-deposited submonolayer of a molecular iron(II) complex *J. Phys. Chem. Lett.* **3** 3431–4
- [11] Rohlf S *et al* 2018 Light-induced spin crossover in an Fe(II) low-spin complex enabled by surface adsorption *J. Phys. Chem. Lett.* **9** 1491–6
- [12] Atzori M, Poggini L, Squillantini L, Cortigiani B, Gonidec M, Bencok P, Sessoli R and Mannini M 2018 Thermal and light-induced spin transition in a nanometric film of a new high-vacuum processable spin crossover complex *J. Mater. Chem. C* **6** 8885–9

- [13] Bernien M *et al* 2015 Highly efficient thermal and light-induced spin-state switching of an Fe(II) complex in direct contact with a solid surface *ACS Nano* **9** 8960–6
- [14] Kipgen L, Bernien M, Nickel F, Naggert H, Britton A J, Arruda L M, Schierle E, Weschke E, Tucek F and Kuch W 2017 Soft-x-ray-induced spin-state switching of an adsorbed Fe(II) spin-crossover complex *J. Phys.: Condens. Matter* **29** 394003
- [15] Kipgen L *et al* 2018 Evolution of cooperativity in the spin transition of an iron(II) complex on a graphite surface *Nat. Commun.* **9** 2984
- [16] Gopakumar T G *et al* 2013 Spin-crossover complex on Au(111): structural and electronic differences between mono- and multilayers *Chem. A Eur. J.* **19** 15702–9
- [17] Decurtins S, Gütllich P, Köhler C P, Spiering H and Hauser A 1984 Light-induced excited spin state trapping in a transition-metal complex: the hexa-1-propyltetrazole-iron(II) tetrafluoroborate spin-crossover system *Chem. Phys. Lett.* **105** 1–4
- [18] Hauser A 2004 Light-induced spin crossover and the high-spin  $\rightarrow$  low-spin relaxation *Spin Crossover in Transition Metal Compounds II (Topics in Current Chemistry vol 234)* (Berlin: Springer) pp 155–98
- [19] Gopakumar T G, Matino F, Naggert H, Bannwarth A, Tucek F and Berndt R 2012 Electron-induced spin crossover of single molecules in a bilayer on gold *Angew. Chem., Int. Ed. Engl.* **51** 6262–6
- [20] Ossinger S *et al* 2017 Vacuum-evaporable spin-crossover complexes in direct contact with a solid surface: bismuth versus gold *J. Phys. Chem. C* **121** 1210–9
- [21] Naggert H, Rudnik J, Kipgen L, Bernien M, Nickel F, Arruda L M, Kuch W, Näther C and Tucek F 2015 Vacuum-evaporable spin-crossover complexes: physicochemical properties in the crystalline bulk and in thin films deposited from the gas phase *J. Mater. Chem. C* **3** 7870–7
- [22] Ossinger S, Naggert H, Bill E, Näther C and Tucek F 2019 Electronic structure, vibrational spectra, and spin-crossover properties of vacuum-evaporable iron(II) bis(dihydrobis(pyrazolyl)borate) complexes with diimine coligands. Origin of giant Raman features *Inorg. Chem.* **58** 12873–87
- [23] Cartier dit Moulin C, Rudolf P, Flank A M and Chen C T 1992 Spin transition evidenced by soft x-ray absorption spectroscopy *J. Phys. Chem.* **96** 6196–8
- [24] Gütllich P and Goodwin H A 2004 Spin crossover—an overall perspective *Spin Crossover in Transition Metal Compounds I (Topics in Current Chemistry vol 233)*, ed P Gütllich and H A Goodwin (Berlin: Springer) pp 1–47
- [25] Real J A, Muñoz M C, Faus J and Solans X 1997 Spin crossover in novel dihydrobis(1-pyrazolyl)borate [H<sub>2</sub>B(pz)<sub>2</sub>]-containing iron(II) complexes. Synthesis, x-ray structure, and magnetic properties of [FeL{H<sub>2</sub>B(pz)<sub>2</sub>}]<sub>2</sub> (L = 1,10-phenanthroline and 2,2'-Bipyridine) *Inorg. Chem.* **36** 3008–13
- [26] Hill A F, Malget J M, White A J P and Williams D J 2004 Dihydrobis(pyrazolyl)borate alkylidyne complexes of tungsten *Eur. J. Inorg. Chem.* **2004** 818–28
- [27] Abernethy R J, Hill A F, Smith M K and Willis A C 2009 Boron functionalization of bis(pyrazolyl)borate ligands: molecular structures of [RuX(PPh<sub>3</sub>)<sub>2</sub>{(MeO)<sub>2</sub>B(pz)<sub>2</sub>}] (X = H, Cl; pz = pyrazol-1-yl) *Organometallics* **28** 6152–9
- [28] Trofimenko S 1967 Boron-pyrazole chemistry. II. Poly(1-pyrazolyl)-borates *J. Am. Chem. Soc.* **89** 3170–7
- [29] Ossinger S, Näther C and Tucek F 2016 Bis[di-hydro-bis-(pyrazol-1-yl- $\kappa$ N<sup>2</sup>)borato]bis(methanol- $\kappa$ O)iron(II) *IUCrData* **1** x161252
- [30] Ossinger S, Näther C and Tucek F 2019 Crystal structure of bis-[di-hydro-bis-(pyrazol-1-yl)borato- $\kappa^2$ N<sup>2</sup>,N<sup>2</sup>] (1,10-phenanthroline- $\kappa^2$ N,N')zinc(II) *Acta Crystallogr. E* **75** 1112–6
- [31] Warner B *et al* 2013 Temperature- and light-induced spin crossover observed by x-ray spectroscopy on isolated Fe(II) complexes on gold *J. Phys. Chem. Lett.* **4** 1546–52
- [32] Pronschinske A, Chen Y, Lewis G F, Shultz D A, Calzolari A, Buongiorno Nardelli M and Dougherty D B 2013 Modification of molecular spin crossover in ultrathin films *Nano Lett.* **13** 1429–34
- [33] Gruber M, Miyamachi T, Davesne V, Bowen M, Boukari S, Wulfhekel W, Alouani M and Beaurepaire E 2017 Spin crossover in Fe(phen)<sub>2</sub>(NCS)<sub>2</sub> complexes on metallic surfaces *J. Chem. Phys.* **146** 92312
- [34] Beniwal S *et al* 2016 Surface-induced spin state locking of the [Fe(H<sub>2</sub>B(pz)<sub>2</sub>)<sub>2</sub>(bipy)] spin crossover complex *J. Phys.: Condens. Matter* **28** 206002
- [35] Gruber M, Davesne V, Bowen M, Boukari S, Beaurepaire E, Wulfhekel W and Miyamachi T 2014 Spin state of spin-crossover complexes: from single molecules to ultrathin films *Phys. Rev. B* **89** 195415
- [36] Fourmental C *et al* 2019 Importance of epitaxial strain at a spin-crossover molecule–metal interface *J. Phys. Chem. Lett.* **10** 4103–9
- [37] Karthikeyan S, Ramanathan V and Mishra B K 2013 Influence of the substituents on the CH... $\pi$  interaction: Benzene–Methane complex *J. Phys. Chem. A* **117** 6687–94